(4)

AD

TECHNICAL REPORT ARCCB-TR-88043

THE BLAST FIELD PRODUCED BY A CANNON HAVING A PERFORATED MUZZLE BRAKE

G. C. CAROFANO

DECEMBER 1988

US ARMY ARMAMENT RESEARCH,
DEVELOPMENT AND ENGINEERING CENTER
CLOSE COMBAT ARMAMENTS CENTER
BENÉT LABORATORIES
WATERVLIET, N.Y. 12189-4050

DISCLAIMER

The findings in this report are not to be construed as an official Department of the Army position unless so designated by other authorized documents.

The use of trade name(s) and/or manufacturer(s) does not constitute an official indorsement or approval.

DESTRUCTION NOTICE

For classified documents, follow the procedures in DoD 5200.22-M, Industrial Security Manual, Section II-19 or DoD 5200.1-R, Information Security Program Regulation, Chapter IX.

For unclassified, limited documents, destroy by any method that will prevent disclosure of contents or reconstruction of the document.

For unclassified, unlimited documents, destroy when the report is no longer needed. Do not return it to the originator.

SECURITY CLASSIFICATION OF THIS PAGE (When Data Entered)

REPORT DOCUMENTATION PAGE

READ INSTRUCTIONS BEFORE COMPLETING FORM

1. REPORT NUMBER: ARCCB-TR-88043	2. GOVT ACCESSION NO.
3. RECIPIENT'S CATALOG NUMBER	
4. TITLE (and Subtitle): THE BLAST FIELD PRODUCED BY A CANNON HAVING A PERFORATED MUZZLE BRAKE	5. TYPE OF REPORT & PERIOD COVERED: Final
6. PERFORMING ORG. REPORT NUMBER	
7. AUTHOR(s): G. C. Carofano	8. CONTRACT OR GRANT NUMBER(s)
9. PERFORMING ORGANIZATION NAME AND ADDRESS: US Army ARDEC, Benet Laboratories, SMCAR-CCB-TL, Watervliet, NY 12189-4050	10. PROGRAM ELEMENT, PROJECT, TASK AREA & WORK UNIT NUMBERS: AMCMS No. 6111.02.H610.011, PRON No. 1A84Z8CAN1SC
11. CONTROLLING OFFICE NAME AND ADDRESS: US Army ARDEC, Close Combat Armaments Center, Picatinny Arsenal, NJ 07806-5000	12. REPORT DATE: December 1988 13. NUMBER OF PAGES: 36
14. MONITORING AGENCY NAME & ADDRESS (if different from Controlling Office)	15. SECURITY CLASS. (of this report): UNCLASSIFIED 15a. DECLASSIFICATION/DOWNGRADING SCHEDULE

16. DISTRIBUTION STATEMENT (of this Report)

Approved for public release; distribution unlimited.

17. DISTRIBUTION STATEMENT (of the abstract entered in Block 20, if different from Report)

18. SUPPLEMENTARY NOTES

Presented at the Fifty-Ninth Shock and Vibration Symposium, Albuquerque, NM, 18-20 October 1988.
Published in Proceedings of the Symposium.

19. KEY WORDS (Continue on reverse side if necessary and identify by block number)

Muzzle Brakes
Perforated Muzzle Brake
Internal Ballistics
Muzzle Blast

20. ABSTRACT (Continue on reverse side if necessary and identify by block number)

In a study of perforated muzzle brakes, Nagamatsu, Choi, Duffy, and Carofano calculated the three-dimensional steady flow through one vent hole and used the results to predict overall brake performance. In the present study, the analysis is extended to the calculation of the blast field. The results compare favorably with previously unpublished shadowgraphs obtained by Dillon in his experimental program.

DD FORM 1 JAN 73 1473 EDITION OF 1 NOV 65 IS OBSOLETE

UNCLASSIFIED

SECURITY CLASSIFICATION OF THIS PAGE (When Data Entered)

TABLE OF CONTENTS

TABLES

LIST OF ILLUSTRATIONS

ACKNOWLEDGEMENT

The author would like to thank Major Robert E. Dillon, Jr. for supplying the shadowgraphs from his experiments. They are an essential part of the report.

INTRODUCTION

A perforated muzzle brake consists simply of a set of vents drilled through the wall of a cannon near the muzzle (see Figure 1). Compared with conventional baffle brakes, they are lighter and simpler to manufacture and, as shown in a series of reports by Dillon and Nagamatsu (refs 1-5), they can be designed to provide significant levels of recoil reduction. Also, because the vented area can be located symmetrically around the tube, a more favorable flow environment is provided for finned projectiles. Asymmetrical venting can lead to bending and even breakage of the fins.

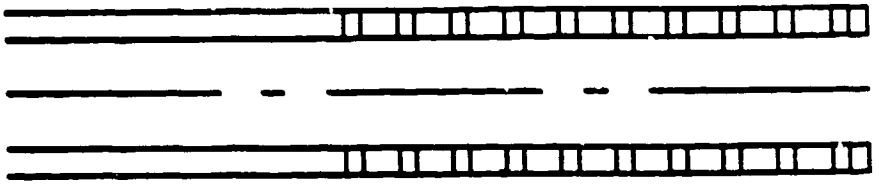

Figure 1. Schematic drawing of a perforated muzzle brake.

Nagamatsu, Duffy, Choi, and Carofano (ref 6) calculated the steady three-dimensional flow through a single vent in the wall of a shock tube. The predicted pressure distribution on the vent wall compared favorably with the experimental measurements of Nagamatsu, Duffy, and Choi (ref 7). It was also shown that these results could be combined with a one-dimensional model of the transient flow in a cannon to predict the impulse reduction produced by a perforated muzzle brake. The predictions agreed well with the experimental measurements of Dillon (ref 1) for a 20-mm cannon. A more comprehensive comparison of the theory with these experiments, including a discussion of brake efficiency and scaling, was made by Carofano (ref 8).

References are listed at the end of this report.

The transient development of the three-dimensional flow through a conventional baffle brake is discussed by Wang, Widhopf, and Chen (ref 9).

In the present study, the analysis is extended to the calculation of the blast field. The complex transient three-dimensional problem is reduced to a one-dimensional flow inside the tube coupled to an axisymmetric model outside. The three-dimensional character of the flow through the tube wall is retained, however, by treating it as quasi-steady. The results are compared with previously unpublished shadowgraphs obtained by Dillon in his experimental program.

THE VENT FLOW FIELD

When the propellant gas expands through the brake, an asymmetric pressure distribution develops in each hole with the highest pressures acting on the downstream surface. The vector and pressure contour plots of Figures 2 and 3 show typical flow patterns in the symmetry plane of one hole and the portion of the tube associated with it. The flow variables in the tube are uniform across the entrance plane. The solid lines in the vector plot indicate where the local Mach number is unity.

In Figure 2, the flow enters at Mach one and accelerates to supersonic velocities as a portion of the gas expands and turns into the hole. The shock at the downstream lip of the hole turns the expanded flow parallel to the solid surfaces and reduces the velocities to subsonic levels. The pressure on the lip is nearly twice the static pressure of the incoming stream. The flow accelerates away from this region and leaves the tube and hole at supersonic velocities. There is a large subsonic region in the upstream portion of the hole. A more complete description of the flow and a comparison with shock tube data are given in Reference 6.

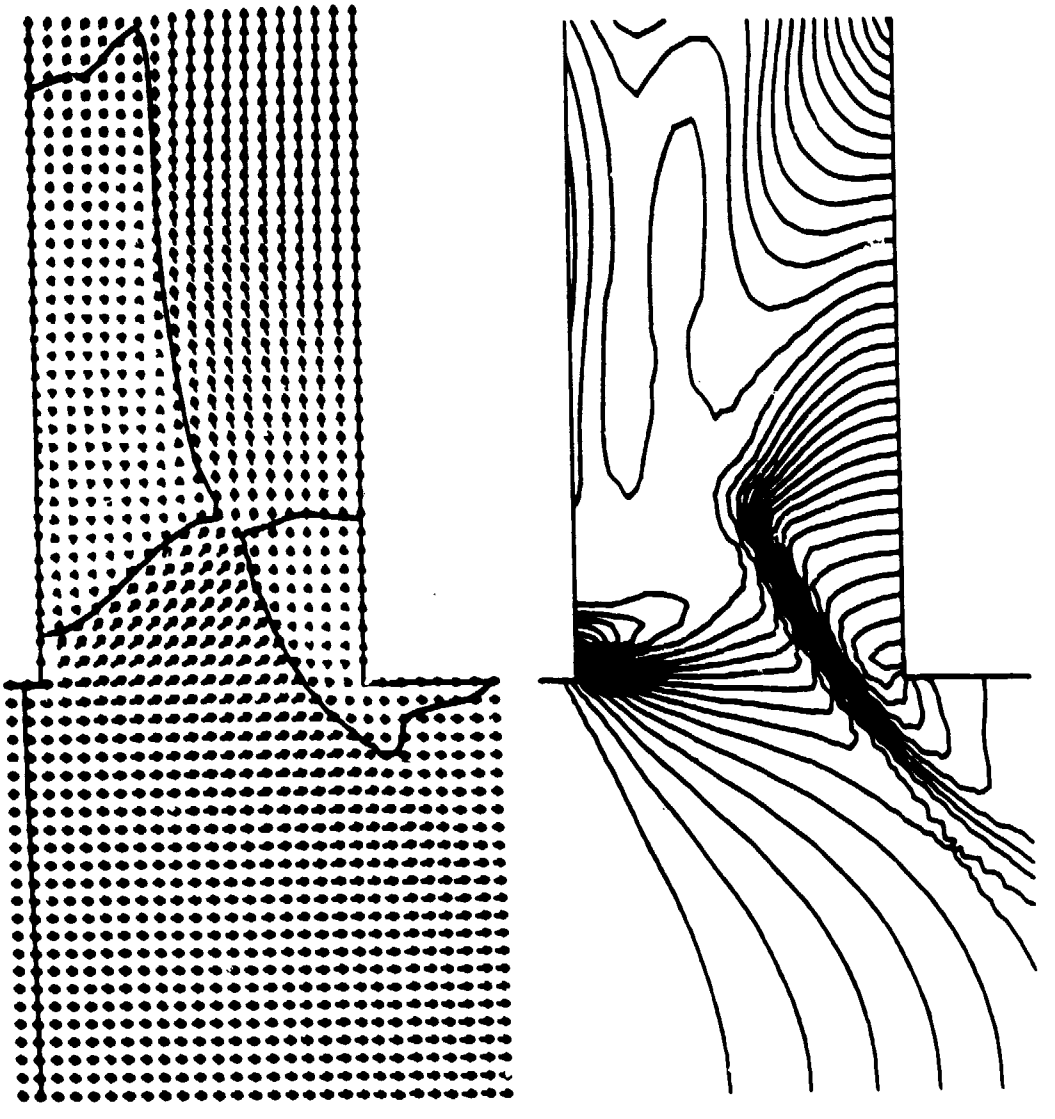

Figure 2. Velocity vector and pressure contour plots for a vent flow with a Mach number of unity at the entrance plane.

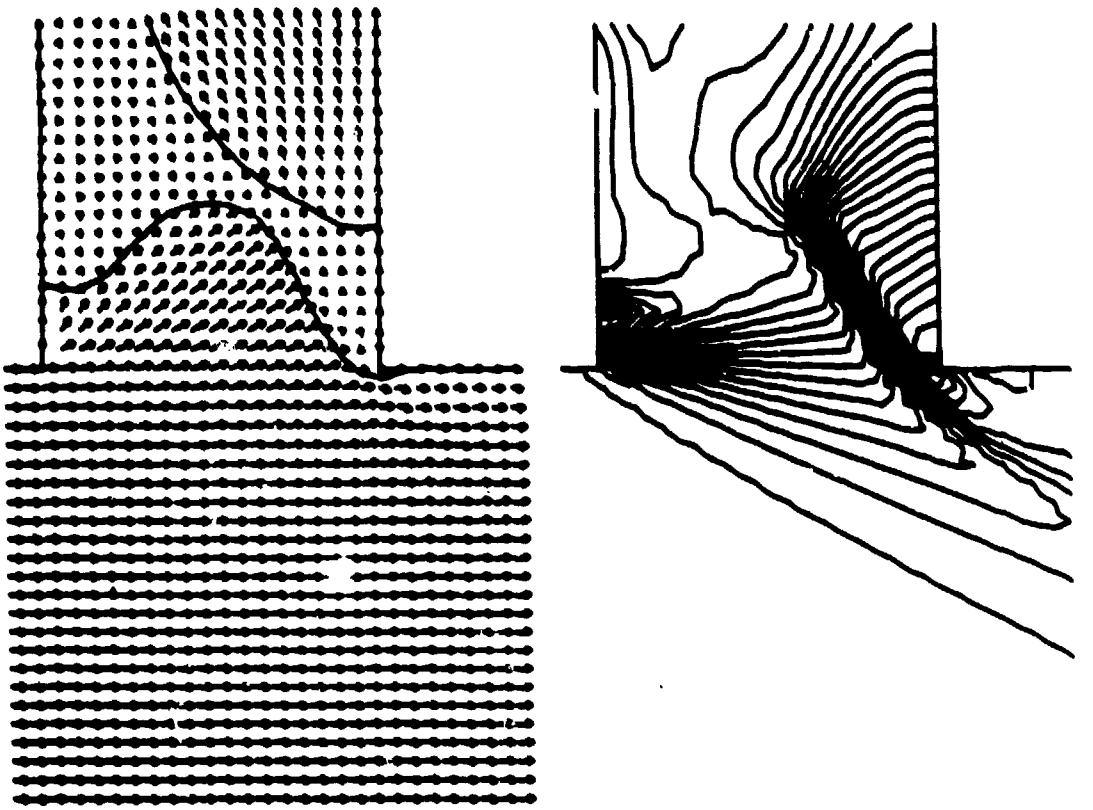

Figure 3. Velocity vector and pressure contour plots for a vent flow with a Mach number of two at the entrance plane.

To calculate the blast field, the flow through each vent is required at each instant of time during tube blowdown. Because the flow is three-dimensional, it is not practical to obtain the complete solution with a transient calculation. Fortunately, the flow contains many features which permit a vigorous simplification of the problem.

First, because of the large volume of the gun tube, the blowdown process takes on the order of tens of milliseconds, while the three-dimensional calculations indicate that the flow in a hole is established in a fraction of a millisecond. Therefore, the latter can be treated as quasi-steady and only the flow inside and outside of the tube must be considered as time-dependent.

Secondly, in the applications of interest, the flow is either sonic or supersonic as it enters the brake and, due to the venting, expands to higher Mach numbers as it travels downstream. Also, because of the high tube pressures, the gas exits each hole at near sonic or supersonic velocities over most of the exit plane area (see Figures 2 and 3). Experience has shown that the flow is rather insensitive to the outflow boundary condition over the remaining subsonic portion. Thus, the flow at a particular hole location is not influenced by events occurring farther downstream or outside of the tube. It depends solely on the conditions in the tube upstream of the hole.

The Euler equations may be written in conservative form as

$$\frac{\partial Q}{\partial t} + \frac{\partial F}{\partial x} + \frac{\partial G}{\partial y} + \frac{\partial H}{\partial z} = 0 \tag{1}$$

where

$$Q = \begin{bmatrix} \rho \\ m \\ n \\ \ell \\ E \end{bmatrix}, \quad F = \begin{bmatrix} m \\ m^2/\rho+P \\ mn/\rho \\ m\ell/\rho \\ (E+P)m/\rho \end{bmatrix}, \quad G = \begin{bmatrix} n \\ nm/\rho \\ n^2/\rho+P \\ n\ell/\rho \\ (E+P)n/\rho \end{bmatrix}, \quad H = \begin{bmatrix} \ell \\ \ell m/\rho \\ \ell n/\rho \\ \ell^2/\rho+P \\ (E+P)\ell/\rho \end{bmatrix}$$

ρ is the density; $m = \rho u$, $n = \rho v$, and $\ell = \rho w$ are the momentum components in the x, y, and z directions, respectively; u, v, and w are the corresponding velocity components. P is the pressure and E is the total energy per unit volume defined as

$$E = \rho e + (m^2+n^2+\ell^2)/2\rho \tag{2}$$

where e is the specific internal energy. Both the propellant gas and the air are taken to be perfect gases, so the pressure is related to the state variables ρ and e by the expression

$$P = (\gamma-1)\rho e \tag{3}$$

where γ is the specific heat ratio.

Consider the result of nondimensionalizing the Euler equations in the following way:

$$\rho' = \rho/\rho_2 \quad , \quad m' = m/\sqrt{P_2\rho_2} \quad , \quad n' = n/\sqrt{P_2\rho_2} \quad , \quad \ell' = \ell/\sqrt{P_2\rho_2}$$

$$P' = P/P_2 \quad , \quad E' = E/P_2 \quad , \quad e' = e\rho_2/P_2 \quad , \quad c' = c\sqrt{\rho_2/P_2}$$

$$x' = x/D \quad , \quad y' = y/D \quad , \quad z' = z/D \quad , \quad t' = t\sqrt{P_2/\rho_2}/D$$

where ρ_2 and P_2 are the density and pressure of the uniform flow at the upstream plane of the tube and D is the vent diameter. The form of the Euler and state equations remains unchanged, while the inflow boundary conditions become

$$\rho' = 1 \tag{4}$$

$$m' = \sqrt{\gamma}M_2 \tag{5}$$

$$n' = \ell' \tag{6}$$

$$E' = 1/(\gamma-1) + \gamma M_2^2/2 \tag{7}$$

Since the flow depends only on the inflow boundary conditions, which are completely described by the upstream Mach number, M_2, the specific heat ratio, γ, and the hole geometry, one solution with these parameters specified is valid for all upstream pressures and densities. This observation is central to the success of the analysis because, while a wide range of physical states are encountered during blowdown, only a few three-dimensional solutions are required to describe them.

Data from the three-dimensional solution are used to obtain average values of the density, ρ_H, pressure, P_H, the mass flux, $\rho_H v_H$, and the axial component of the radial momentum flux, $\rho_H v_H u_H$, in the exit plane of the vent using the following expressions:

$$\rho_H = (1/A_H) \int_{A_H} \rho' dA \tag{8}$$

$$P_H = (1/A_H) \int_{A_H} P' dA \tag{9}$$

$$\rho_H v_H = (1/A_H) \int_{A_H} \rho' v' dA \tag{10}$$

$$\rho_H v_H u_H = (1/AH) \int_{A_H} \rho' v' u' dA \tag{11}$$

where u is the velocity component parallel to the tube axis and v is the component parallel to the vent axis. The integration is carried out over the vent exit area, A_H. The fluxes are calculated rather than the velocities because they are used directly to compute the local vent rate in the interior solution and the weapon impulse (ref 8). The averages are dimensionless and are functions of the parameters that appear in the three-dimensional solution. Their use will be described below.

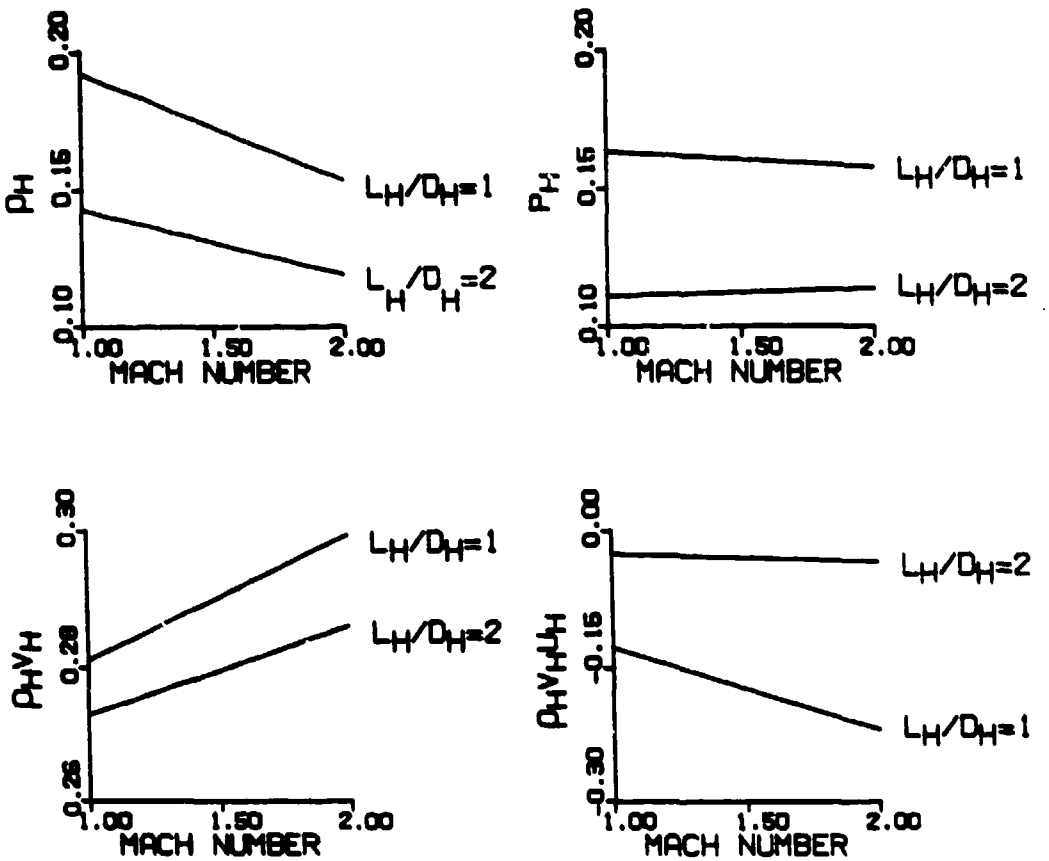

Figure 4. The averaged functions computed from the three-dimensional solutions.

The gas venting through the brake will either be the air ahead of the projectile--the precursor flow--or propellant gas. Experience has shown that the three-dimensional solutions are not particularly sensitive to the value of γ, therefore the numerical results obtained in Reference 8 for $\gamma = 1.22$ were used in this study. The interior and exterior flows are computed using the appropriate specific heat ratios, however.

The averaged functions are shown in Figure 4. The hole geometry is characterized by the ratio of its height, L_H, to its diameter, D_H. The height is equal to the tube wall thickness. Note that the momentum flux is negative for both vent heights, especially the shorter one. This is consistent with the velocity vector plots of Figures 2 and 3--the flow leaving the shorter vent is, on balance, directed more upstream.

THE INTERIOR FLOW FIELD

The flow inside the tube is calculated using the one-dimensional Euler equations with a source term included to represent the venting at the tube wall.

$$\frac{\partial \rho}{\partial t} + \frac{\partial m}{\partial x} = \frac{1}{A}\frac{\dot{dm}}{dx} \tag{12}$$

$$\frac{\partial m}{\partial t} + \frac{\partial (m^2/\rho + P)}{\partial x} = \frac{m}{\rho A}\frac{\dot{dm}}{dx} \tag{13}$$

$$\frac{\partial E}{\partial t} + \frac{\partial (m(E+P)/\rho)}{\partial x} = \frac{(E+P)}{\rho A}\frac{\dot{dm}}{dx} \tag{14}$$

The vent term $(1/A)\dot{dm}/dx$ represents the mass of fluid per unit time per unit volume leaving the tube at x. A is the bore area. The fluid is assumed to leave at the local velocity u in the momentum equation and with the local enthalpy per unit mass $(E+P)/\rho$ in the energy equation (see Reference 10 for the derivation of these equations).

The theory will be compared with an experimental brake having holes of a single diameter and a uniform spacing, S_H, along the tube. The vent area per unit length is $\pi N_C D_H^2/4S_H$ where N_C is the number of holes per row (rows run around the circumference of the tube). The vent term can then be written in dimensional form as

$$(1/A)d\dot{m}/dx = -\rho_H v_H \sqrt{P\rho}(N_C/S_H)(D_H/D_B)^2 \qquad (15)$$

where D_B is the tube diameter. P and ρ are the local values of pressure and density in the one-dimensional solution; they appear since these quantities were used to nondimensionalize the product $\rho_H v_H$ in the three-dimensional solution. The latter is also a function of the local Mach number.

THE EXTERIOR SOLUTION

The flow outside of the tube is treated as axisymmetric. The large number of vents typical of such brakes and their symmetrical placement around the tube makes this feasible. The Euler equations take the following form:

$$\frac{\partial Q}{\partial t} + \frac{\partial F}{\partial x} + \frac{\partial G}{\partial y} + W = 0 \qquad (16)$$

where

$$Q = \begin{bmatrix} \rho \\ m \\ n \\ E \\ S \end{bmatrix}, \quad F = \begin{bmatrix} m \\ m^2/\rho+P \\ mn/\rho \\ (E+P)m/\rho \\ Sm/\rho \end{bmatrix}, \quad G = \begin{bmatrix} n \\ nm/\rho \\ n^2/\rho+P \\ (E+P)n/\rho \\ Sn/\rho \end{bmatrix}, \quad W = \frac{n}{y}\begin{bmatrix} 1 \\ m/\rho \\ n/\rho \\ (E+P)/\rho \\ S/\rho \end{bmatrix}$$

Since two gases are present, the state variables must be evaluated for a mixture. The details are fully explained in Rererence 11. The last equation in this set is a species equation where S represents the mass concentration of the air at a particular location.

At the muzzle, the one-dimensional equations are solved simultaneously with the axisymmetric equations downstream. The remainder of the tube is a solid boundary except for the vented region. Since the area of each vent represents only a portion of the local tube area, the averaged variables at the vent exit have to be adjusted to provide an appropriate boundary condition for the axisymmetric equations.

The sketch in Figure 5 represents a cross section through the vented region of the tube along a plane parallel to the tube axis. Three rows of holes are shown. The center row has an annular control volume drawn above it which extends completely around the circumference of the tube. The width of the control volume is the hole spacing, S_H, and its height is δ. If δ is allowed to approach zero, then the only relevant flux vector in Eq. (16) is G(Q). The flow adjusts instantaneously from the smaller vent exit area, A_H, to the larger tube surface area $A_S = \pi(D_B + 2L_H)S_H/N_C$. Writing this balance out gives

$$\rho_H v_H A_H = \rho_S v_S A_S \tag{17}$$

$$P_a(A_S - A_H) + (\rho_H v_H^2 + P_H)A_H = (\rho_S v_S^2 + P_S)A_S \tag{18}$$

$$\rho_H v_H u_H A_H = \rho_S v_S u_S A_S \tag{19}$$

$$(E_H + P_H)v_H A_H = (E_S + P_S)v_S A_S \tag{20}$$

The species equation is not written out since the vented gas will either be air with $S_S = \rho_S$ or propellant gas with $S_S = 0$.

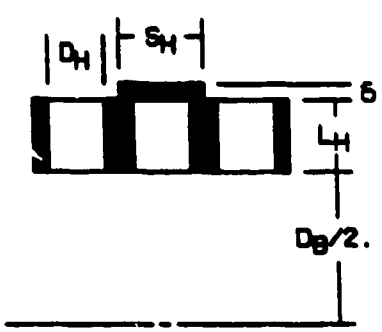

Figure 5. Control volume used to construct the boundary conditions along the vented portion of the tube.

The first term on the left-hand side of the axial momentum equation represents some average pressure, P_a, acting on the area difference $(A_S - A_H)$. Since this pressure is not known, it will be assumed that the gas undergoes an isentropic expansion so that this equation can be replaced with the expression

$$P_S/P_H = (\rho_S/\rho_H)^{\gamma} \tag{21}$$

where γ is appropriate to the gas being vented. With a little algebra, the following results are obtained:

$$M_S = M_H \frac{A_H}{A_S} \left[\frac{2 + (\gamma-1)M_H^2}{2 + (\gamma-1)M_S^2}\right]^{\frac{1}{2}\frac{(\gamma+1)}{(\gamma-1)}} \tag{22}$$

$$\rho_S = \rho_H \left[\frac{M_H A_H}{M_S A_S}\right]^{2/(\gamma+1)} \tag{23}$$

$$v_S = v_H(\rho_H A_H/\rho_S A_S), \qquad u_S = u_H \tag{24}$$

where $M = u/\sqrt{\gamma P/\rho}$. After determining M_S by iteration, the conserved variables in the Euler equations can be formed. The quantities at the vent exit are related to the interior flow through the averaged functions given above. Because the vent exit flow is supersonic, the exterior boundary condition is completely determined by the local conditions in the tube.

Harten's Total Variation Diminishing scheme (ref 12) was used in conjunction with a time-splitting algorithm to solve the Euler equations. A more thorough description of the numerical methods is given in References 6 and 11.

THE STARTING SOLUTION

The first two configurations of Reference 1 will be analyzed: the bare muzzle case and brake #1. This brake has 16 rows of holes arranged in a staggered pattern with every other row of 12 holes rotated 15 degrees with respect to the adjacent rows. The holes are drilled perpendicular to the tube

axis. The brake adds 11.84 cm to the length of the cannon. A more complete description of the experimental setup, including photographs of the brakes, is given in Reference 1. The data in Table I are also taken from that source.

TABLE I. INITIAL DATA FOR 20-MM CANNON

P_m = 287.0 atm	U = 41.7 cm^3	γ_p = 1.25
V_m = 1045.0 m/sec	C = 0.0389 kg	M_p = 22.8
T_L = 143.0 cm	W = 0.098 kg	D_H = 0.0579 cm
L_p = 7.5 cm	γ_a = 1.40	S_H = 0.0866 cm
D_B = 2.00 cm	M_a = 29.0	L_H = 0.0709 cm

P_m and V_m are the measured projectile base pressure and velocity, respectively, at the muzzle exit plane. T_L is the projectile travel length, L_p is the projectile length, D_B is the bore diameter, U is the chamber volume, C is the charge mass, and W is the projectile mass. γ is the specific heat ratio and M is the molecular weight of the gases; the subscripts "a" and "p" refer to the air and propellant gas, respectively.

The starting configurations are shown schematically in Figure 6. The overall length of 156.3 cm in the bare muzzle case includes a uniform extension of the tube to account for the chamber volume. The projectile velocity is kept constant throughout the calculation.

Initially, the projectile nose is 21.8 cm from the muzzle with the precursor shock at the muzzle exit plane. This distance places the precursor shock at the correct position in the first shadowgraph to be presented below. The state of the air ahead of the projectile corresponds to a shock Mach number based on the ratio of the projectile velocity to the acoustic speed in the stagnant environment. This method of introducing the precursor flow into the calculation underestimates the mass of air expelled from the weapon which is $(T_L-L_p)A\ \rho_e$.

ρ_e is the density of the environment. In the computation, the 21.8-cm air column has a density of 4.52 ρ_e. Taking the ratio of the two masses shows that 38 percent more air is expelled by the weapon. The deficiency could be corrected by using a projectile travel-time curve from an internal ballistics code to generate the precursor flow from shot start, but the computation time would also increase significantly. The effect of the precursor flow on the blast field will be explored below. Identical starting conditions were used when the brake was added, as indicated in Figure 6

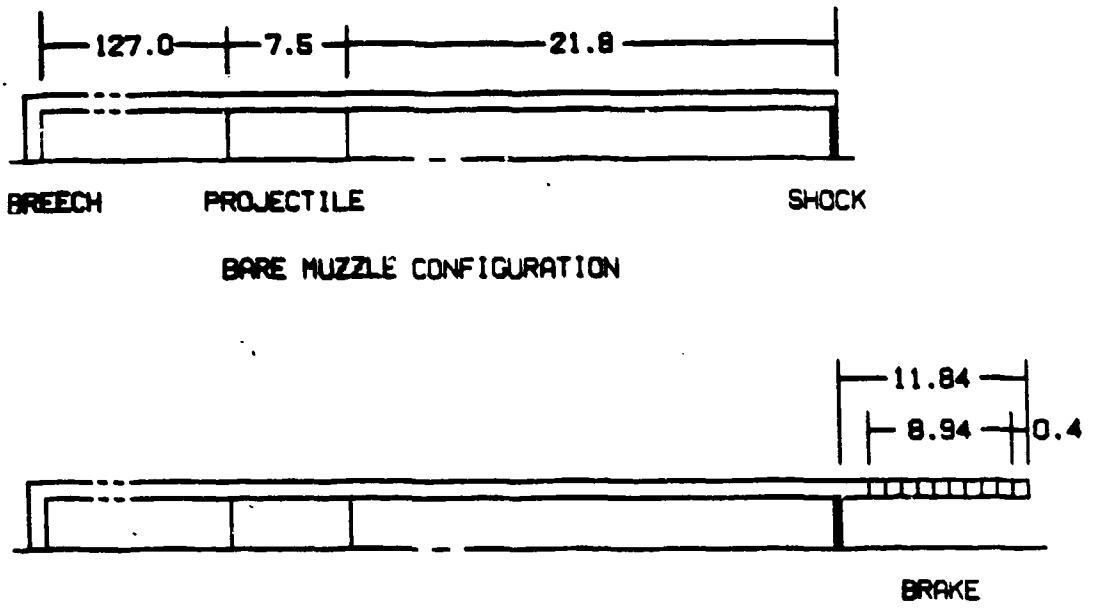

Figure 6. The starting configurations with and without the brake. All dimensions are in centimeters.

The calculation proceeds until the projectile base reaches the position of the bare muzzle exit plane. At this instant, the state of the propellant gas behind the projectile is computed from the information in Table I. The distributions of pressure, density, and velocity are based on the Pidduck-Kent limiting solution (ref 13) specialized to a perfect gas. These are given by

$$\Omega = \frac{(\gamma-1)}{2\gamma}\frac{C}{W}\left(\frac{(\gamma-1)}{2\gamma}\frac{C}{W} + \int_0^1 \left(\frac{1-\Omega\mu^2}{1-\Omega}\right)^{1/(\gamma-1)} d\mu\right)^{-1} \quad (25)$$

$$X_s = (T_L + U/A) \quad (26)$$

$$X = x/X_s \quad (27)$$

$$P = P_m \left[\frac{1 - \Omega X^2}{1 - \Omega}\right]^{\gamma/(\gamma-1)} \quad (28)$$

$$\rho = \frac{C}{U}\frac{2\gamma}{(\gamma-1)}\frac{\Omega}{(1-\Omega)}\frac{W}{C}\left[\frac{1 - \Omega X^2}{1 - \Omega}\right]^{1/(\gamma-1)} \quad (29)$$

$$u = XV_m \quad (30)$$

Ω is obtained by solving Eq. (25) by iteration. X_s is the projectile base position which includes the uniform chamber volume extension. It remains unchanged when the brake is added.

RESULTS

A set of five shadowgraphs was obtained for each of the brakes tested by Dillon (ref 1), but they were not included in that report. Some of these shadowgraphs are presented in this section--the rest may be found in the Appendix.

The density contour plot in Figure 7 shows the precursor flow just after the projectile clears the muzzle. As noted earlier, the starting configuration was chosen so that the intersection of the precursor shock with the tube axis would closely match that in this shadowgraph. In all of the contour plots presented, the data were dumped at the instant the projectile reached its position in the corresponding shadowgraph. Thus, what is being compared between a contour plot-shadowgraph pair is the structure of the remainder of the flow field. The computed shock shape and plume size compare reasonably well with the experiment in Figure 7.

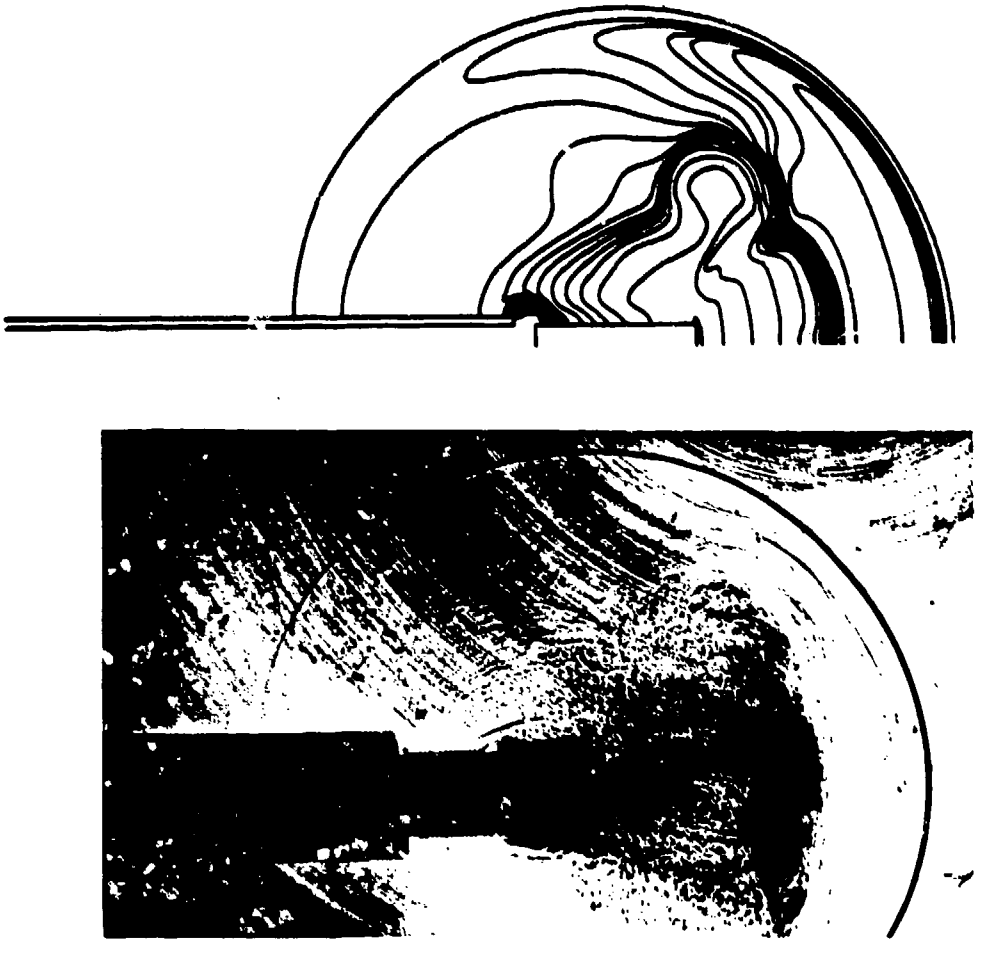

Figure 7. Density contour plot and shadowgraph for the bare muzzle case, t = 0.290 msec.

The shadowgraph in Figure 8 shows that the blast wave does not have the smooth appearance of the precursor shock. The pressure contour plot in the figure also has this feature. It is due to the nonuniform environment generated by the precursor flow. This can be demonstrated by starting the calculation with the projectile nose just upstream of the muzzle, thereby eliminating the precursor flow. The smooth blast wave and simpler plume structure of Figure 9 result. Including the precursor flow increases the computation time by 60 percent, but it appears to be necessary.

The flow field development with the brake in place is depicted in Figures 10 through 12. In the density plot of Figure 10, the expansion of the precursor flow in the tube due to the venting through the brake is evident. It does not appear in Figures 11 and 12 because the contour levels were chosen to emphasize the structure of the exterior flow.

Except for the region where the blast wave intersects the tube wall, the geometries of the precursor and main shocks show good agreement with those in the shadowgraphs. The weak shocks resulting from the interaction of the brake-driven and muzzle-driven portions of the flow are also captured nicely. Unfortunately, the dense propellant gas conceals the rich structure of the plumes in the shadowgraphs.

Perhaps the most intriguing feature in the figures is that the primary thrust of the brake flow is directed considerably rearward even though the holes are drilled perpendicular to the tube axis. This is the result of the expansion of the propellant gas remaining in the tube as it passes the vented region. The pressure drop along the tube axis, shown in Figure 13, is considerable. Also shown in this figure is the pressure distribution along the outside surface of the tube, that is, the boundary condition P_S in Eq. (21). P_S depends directly

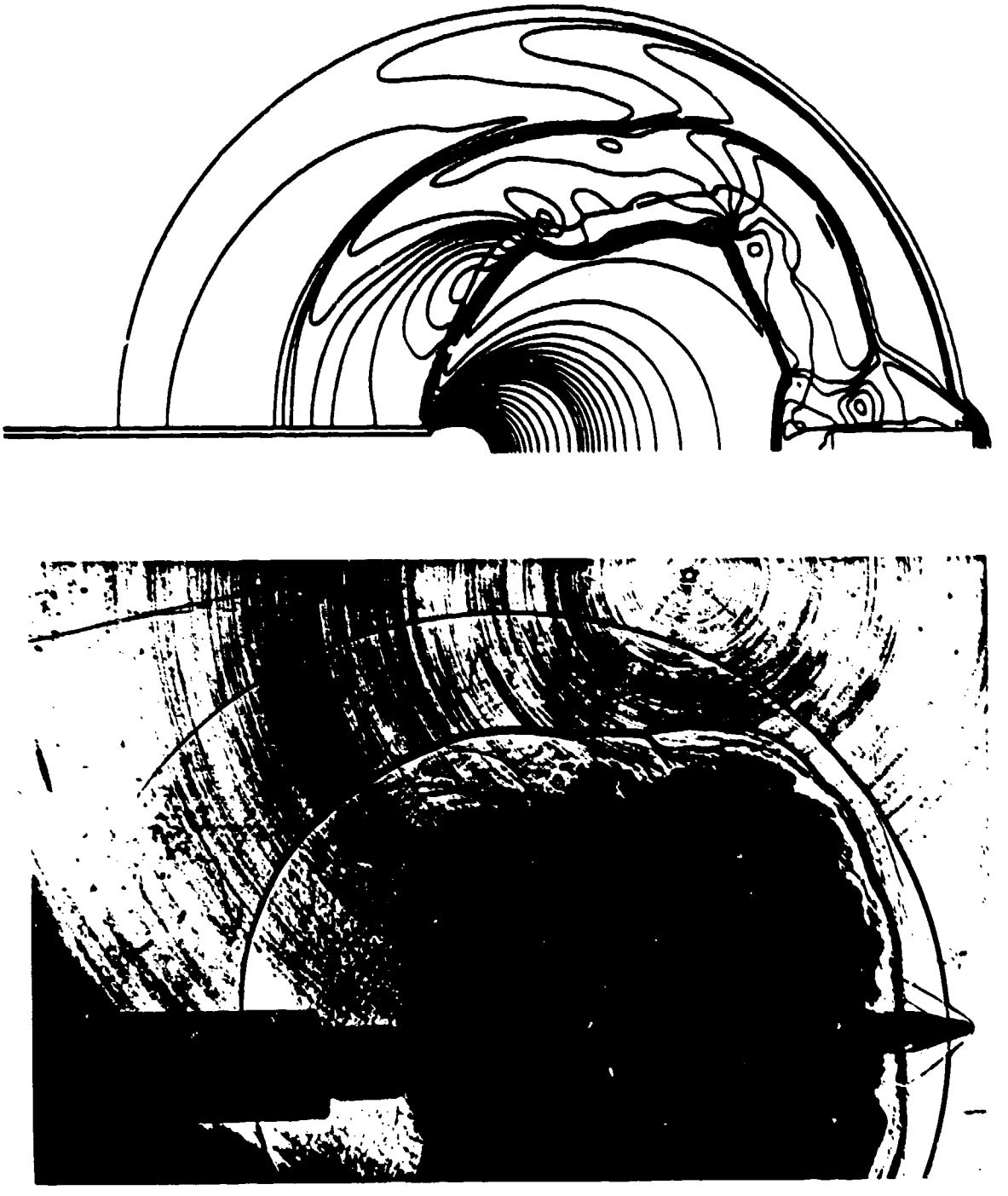

Figure 8. Pressure contour plot and shadowgraph for the bare muzzle case, t = 0.497 msec.

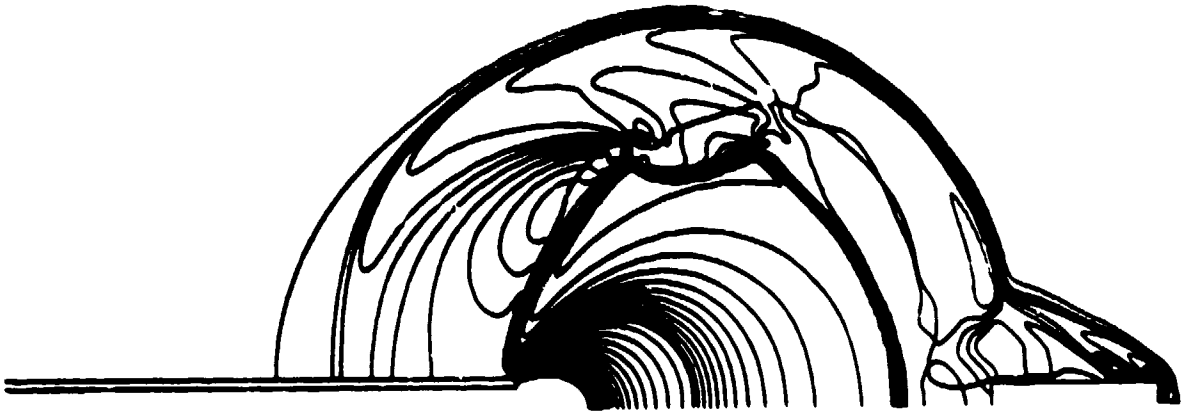

Figure 9. Pressure contour plot for the bare muzzle case with precursor flow eliminated.

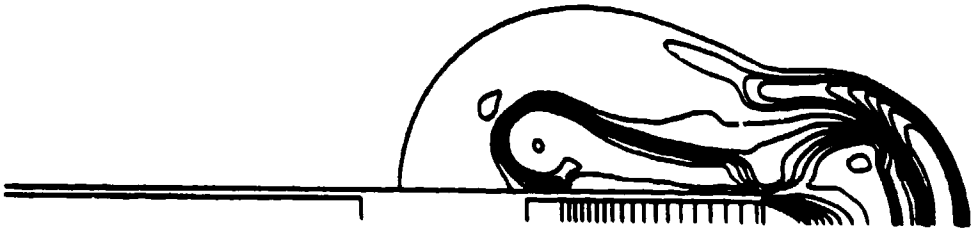

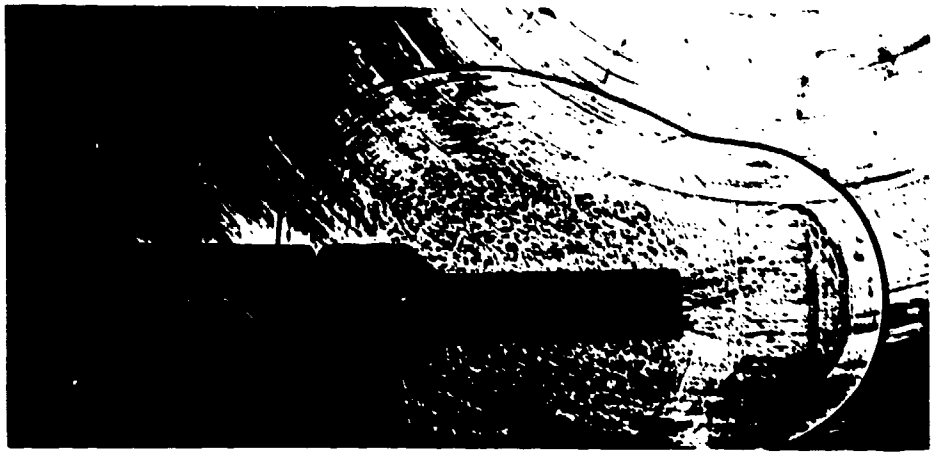

Figure 10. Density contour plot and shadowgraph for the brake case, t = 0.213 msec.

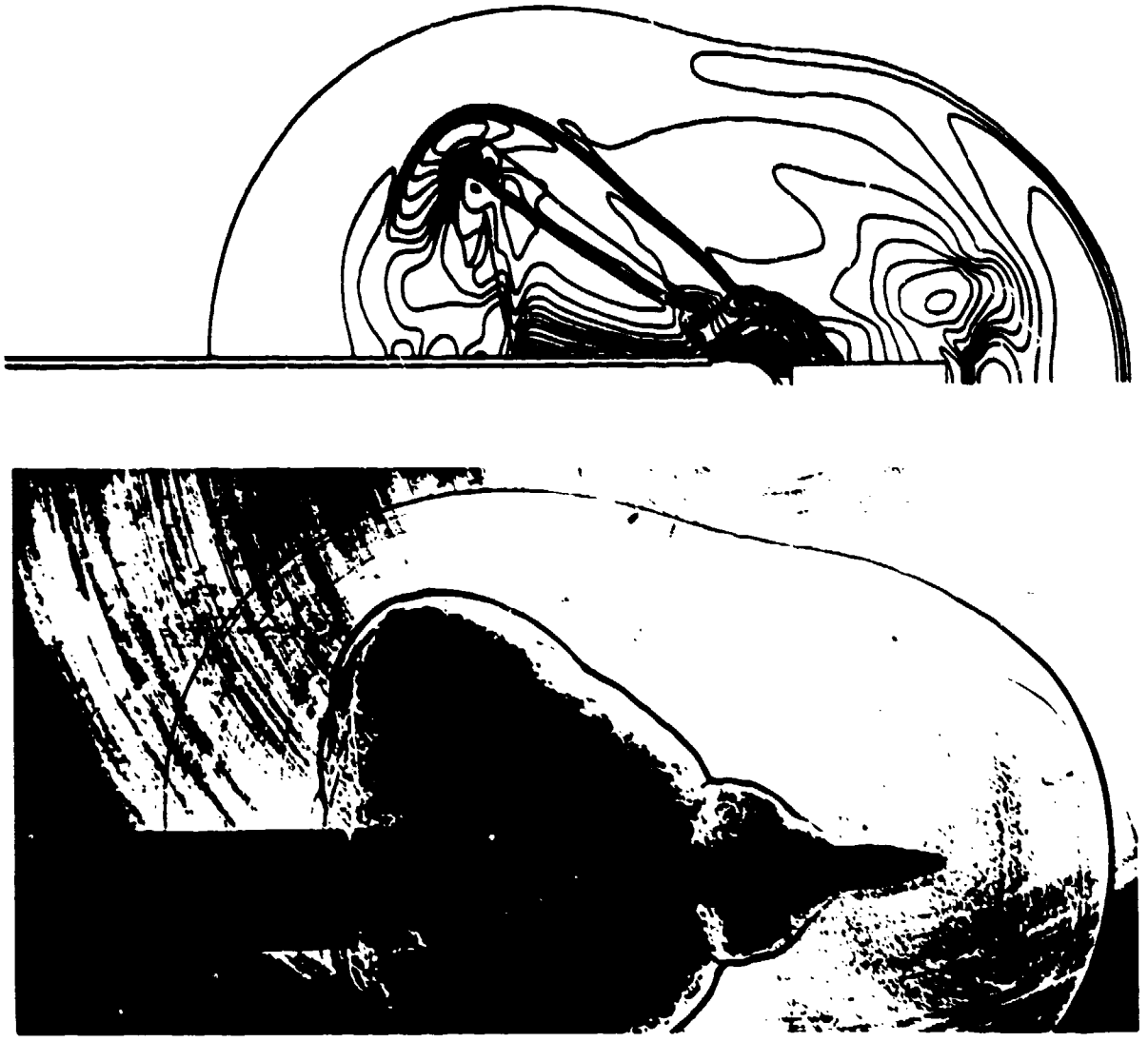

Figure 11. Pressure contour plot and shadowgraph for the brake case, t = 0.423 μsec.

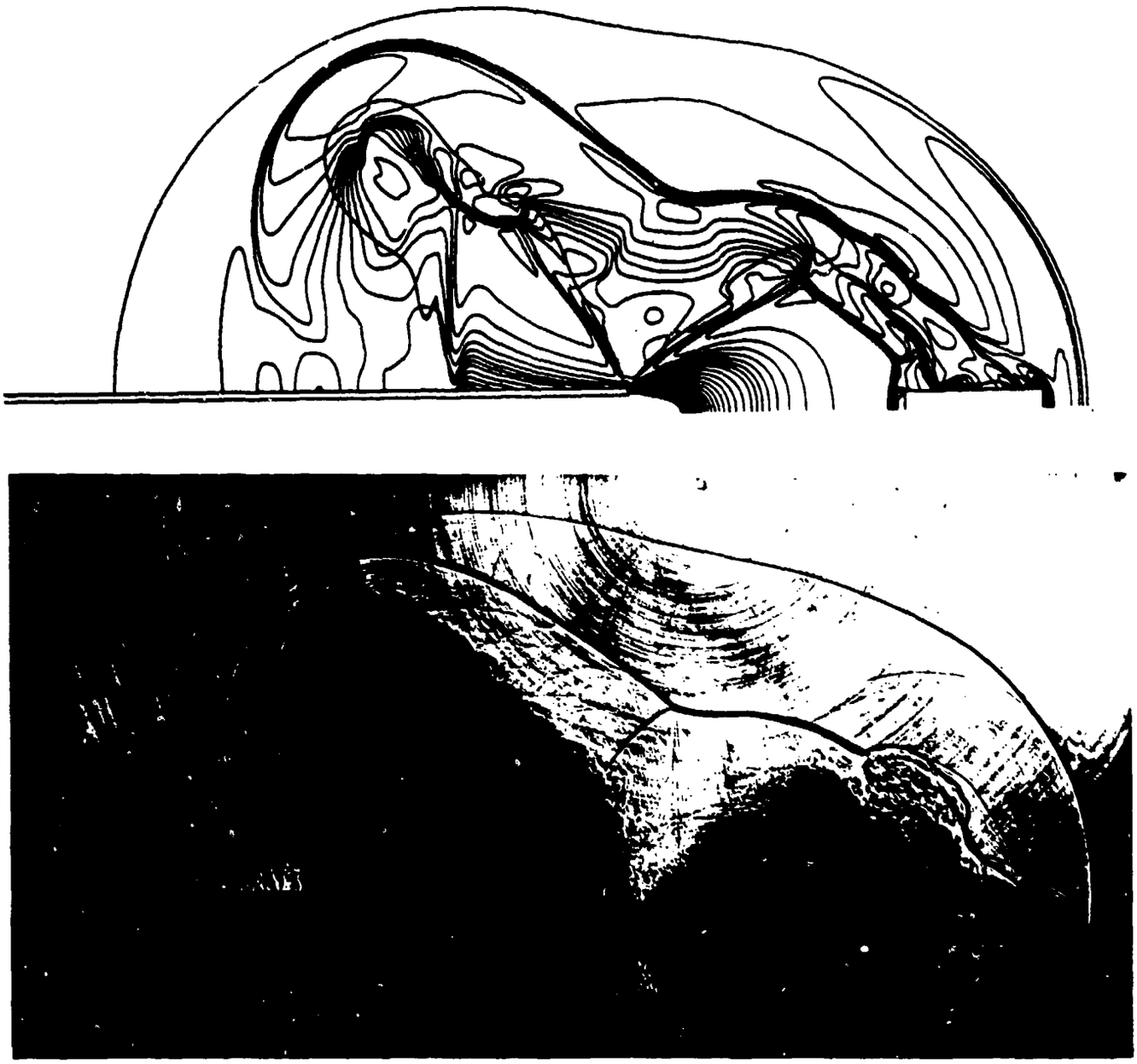

Figure 12. Pressure contour plot and shadowgraph for the brake case, t = 0.546 msec.

on the tube pressure, so its variation with distance is geometrically similar to that in the tube. It is well above atmospheric pressure at the upstream end of the brake, but only slightly above it at the downstream end. Relative to the pressure level between the plume boundary and the main blast wave, the gas at the upstream end of the brake is underexpanded, while that at the downstream is overexpanded.

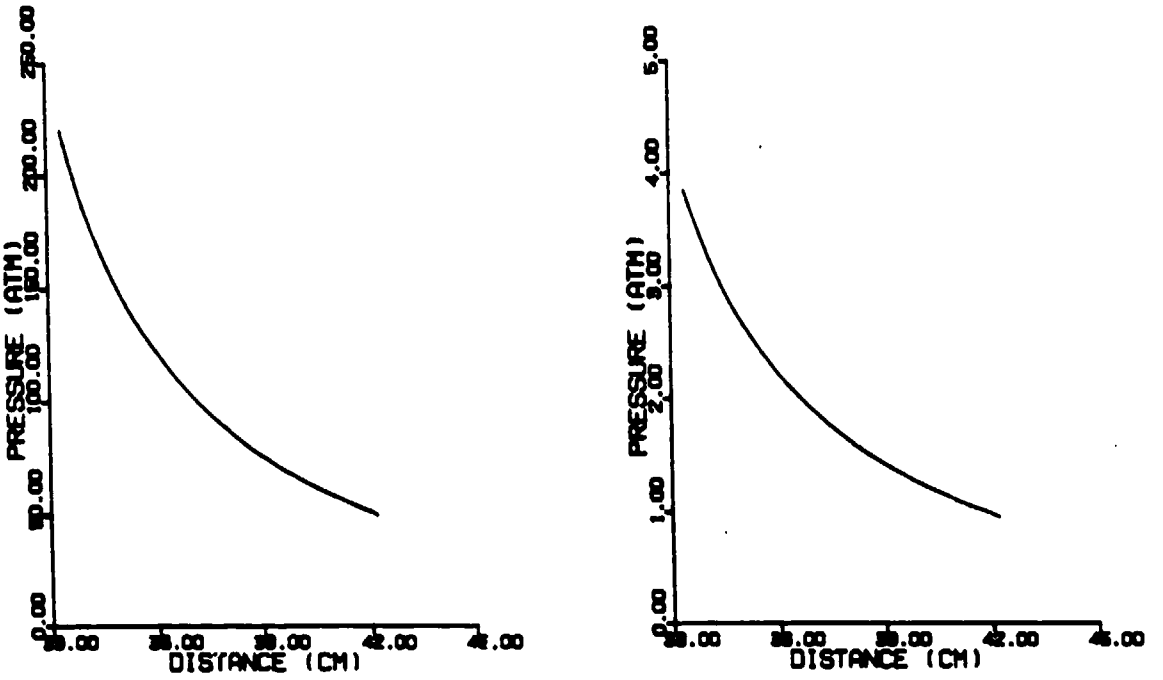

Figure 13. Pressure distribution on the tube axis through the vented region (left) and outside of the brake (right), t = 0.546 msec.

The velocity plot in Figure 14 shows the motion of the propellant gas within the plume. Every fourth vector is plotted to render some clarity to the figure. The plume boundaries are indicated by the solid lines which are actually a plot of the mass fraction of air with contour levels spaced closely around 0.5. They also appear in the pressure plots.

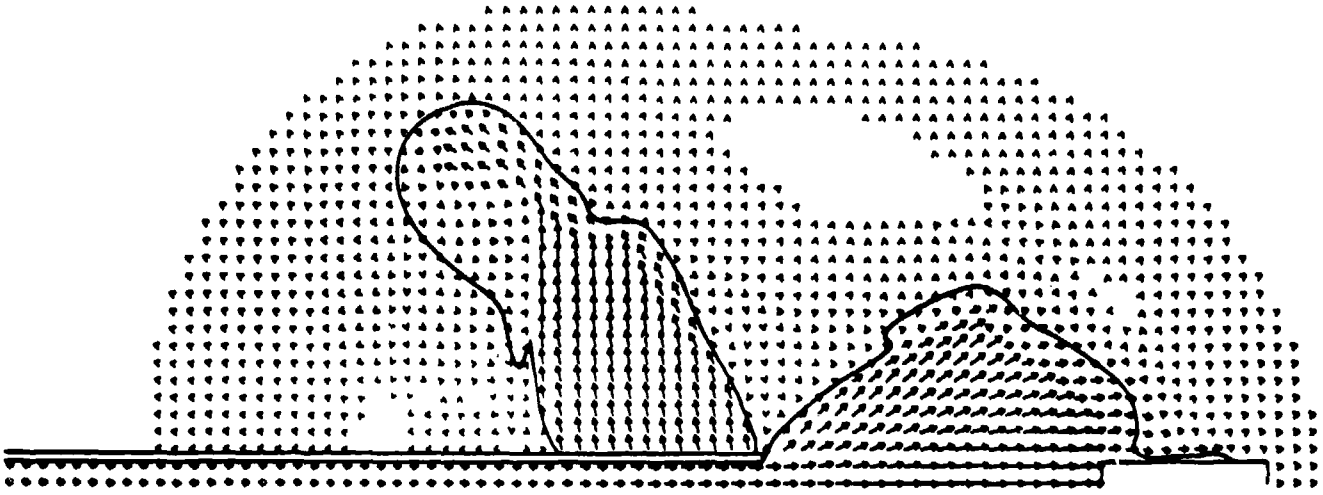

Figure 14. Velocity vector plot for the brake case, t = 0.546 msec.

The vectors indicate that the gas leaves the brake with a slight upstream bias over most of its length. At the upstream end, the underexpanded flow is gradually turned nearly perpendicular to the tube by a weak compression shock. At the downstream end, the overexpanded flow is turned immediately upstream by a compression shock. The shock system which terminates the supersonic flow in the plume also turns the flow upstream. It then undergoes an expansion near the top of the plume where the flow is turned nearly parallel to the tube axis. This expansion is terminated by another shock and the flow then circulates around a large vortex on the left side of the plume. Note the absence of a vortex on the right side.

To determine the influence of the muzzle flow on the shape of the brake plume, the calculation was repeated with the muzzle moved farther downstream. The pressure plot in Figure 15 shows that the brake plume develops essentially as before.

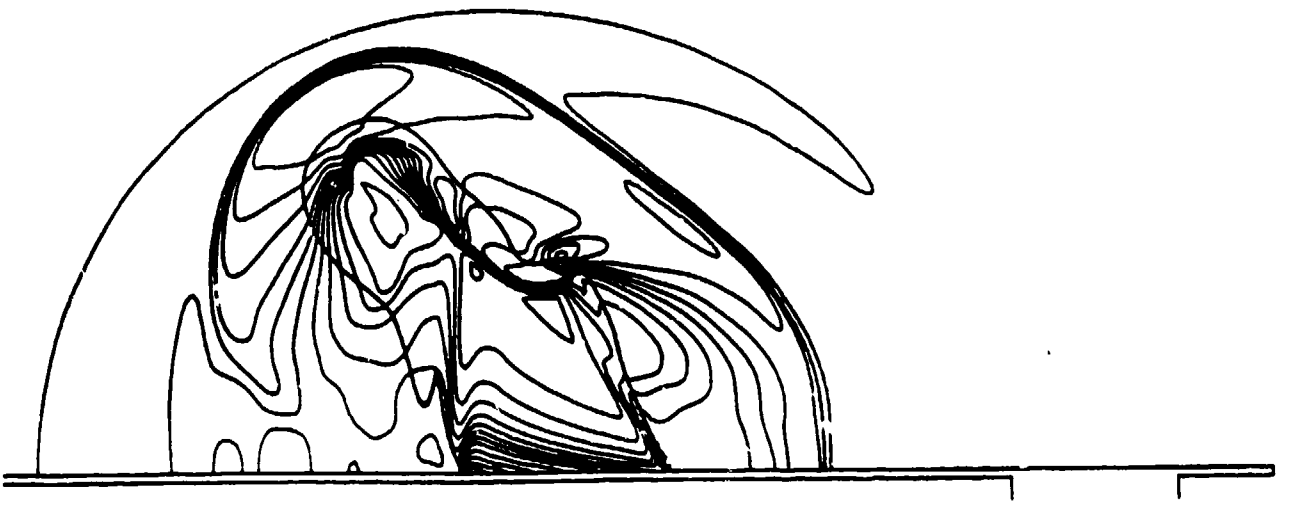

Figure 15. Pressure contour plot for the brake case with muzzle flow removed, t = 0.546 msec.

Removing the precursor flow by placing the projectile nose just upstream of the brake at the start of the calculation produced the result in Figure 16. The plume shape is modified only slightly. It is interesting, however, that now the upstream portion of the blast wave more closely resembles the shadowgraph. This suggests that it may be important to include the full development of the precursor flow from shot start to obtain proper results in this region. It should also be mentioned that failure to include the 45-degree ramp on the tube exterior just upstream of the experimental brake (see shadowgraph in Figure 10) might contribute to the poor agreement, although the corresponding step in the bare muzzle case (see Figure 7) does not seem to influence either the precursor or the main shock development there.

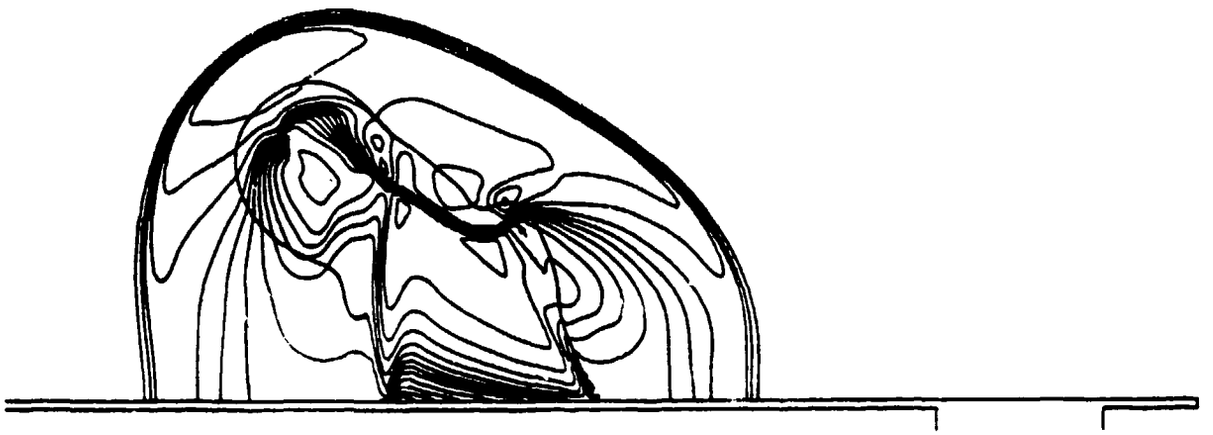

Figure 16. Pressure contour plot for the brake case with muzzle and precursor flows removed, t = 0.546 msec.

CONCLUSIONS

In general, the predicted results compare favorably with the shadowgraphs. The coupling of the interior and exterior flows using a control volume model to make the transition appears to be practical. Perhaps more attention should be paid to the development of the precursor flow.

REFERENCES

1. R. E. Dillon, Jr., "A Parametric Study of Perforated Muzzle Brakes," Technical Report ARLCB-TR-84015, Benet Weapons Laboratory, Watervliet, NY, May 1984.

2. R. E. Dillon, Jr. and H. T. Nagamatsu, "An Experimental Study of Perforated Muzzle Brakes," Technical Report ARLCB-TR-84004, Benet Weapons Laboratory, Watervliet, NY, February 1984.

3. R. E. Dillon, Jr. and H. T. Nagamatsu, "A Method of Analyzing Perforated Muzzle Brake Performance," Technical Report ARLCB-TR-84002, Benet Weapons Laboratory, Watervliet, NY, February 1984.

4. R. E. Dillon, Jr., "Wall Thickness and Vent Area Effects on Perforated Muzzle Brake Performance," Technical Report ARLCB-TR-84020, Benet Weapons Laboratory, Watervliet, NY, June 1984.

5. R. E. Dillon, Jr. and H. T. Nagamatsu, "An Experimental Study of Perforated Muzzle Brakes," AIAA Paper 84-1642, presented at the AIAA 17th Fluid Dynamics, Plasma Dynamics, and Lasers Conference, June 25-27, 1984, Snowmass, CO.

6. H. T. Nagamatsu, K. Y. Choi, R. E. Duffy, and G. C. Carofano, "An Experimental and Numerical Study of the Flow Through a Vent Hole in a Perforated Muzzle Brake," Technical Report ARCCB-TR-87016, Benet Weapons Laboratory, Watervliet, NY, June 1987.

7. H. T. Nagamatsu, K. Y. Choi, and R. E. Duffy, "Wall Thickness and Flow Mach Number Effects on Pressure Distribution in the Vent Hole for Perforated Muzzle Brakes," ARDEC Contractor Report ARCCB-CR-86038, Rensselaer Polytechnic Institute, Troy, NY, November 1986.

8. G. C. Carofano, "The Gasdynamics of Perforated Muzzle Brakes," Technical Report ARCCB-TR-88006, Benet Laboratories, Watervliet, NY, February 1988.

9. J. C. T. Wang, G. F. Widhopf, and S. H. Chen, "A Three-Dimensional, Finite Volume TVD Scheme for Geometrically Complex Steady and Transient Flows," AIAA Paper 88-0228, presented at the AIAA 26th Aerospace Sciences Meeting, January 11-14, 1988, Reno, NV.

10. M. J. Zucrow and J. D. Hoffman, Gas Dynamics - Volume 2: Multidimensional Flow, John Wiley and Sons, New York, 1977, Chapter 19.

11. G. C. Carofano, "Blast Computation Using Harten's Total Variation Diminishing Scheme," Technical Report ARLCB-TR-84029, Benet Weapons Laboratory, Watervliet, NY, October 1984.

12. A. Harten, "High Resolution Schemes for Hyperbolic Conservation Laws," J. Computational Physics, Vol. 49, No. 3, March 1983, pp. 357-393.

13. J. Corner, Theory of the Interior Ballistics of Guns, John Wiley and Sons, New York, 1950.

APPENDIX

The additional shadowgraphs referred to at the beginning of the Results Section are given below. The data for the first contour plot for each configuration were dumped at the instant the intersection of the precursor shock with the tube axis matched that in the corresponding shadowgraph. This was necessary because the location of the projectile in the tube was not known. In the remaining plots, the projectile posi 'on was used as the reference, as described in the text.

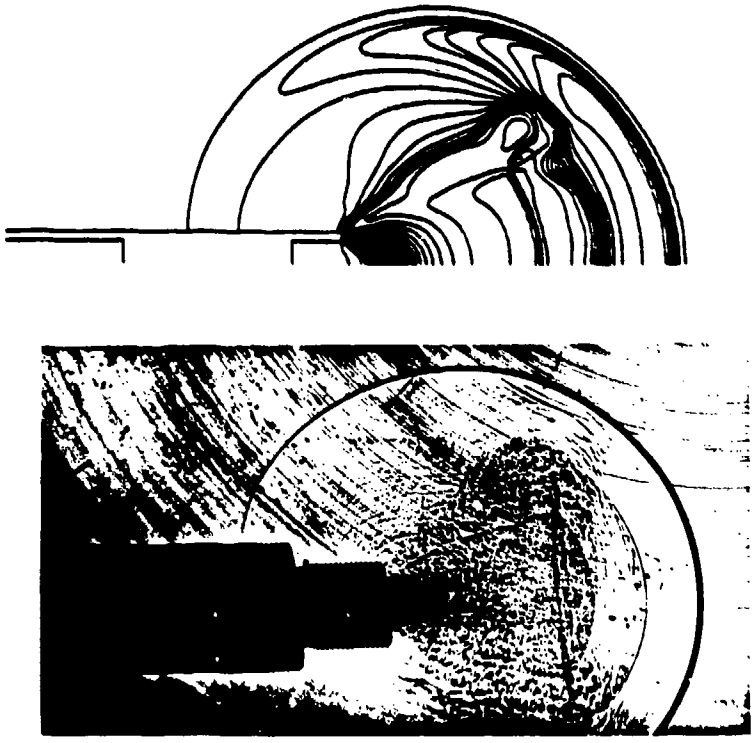

Figure A-1. Density contour plot and shadowgraph for the bare muzzle case, t = 0.187 msec.

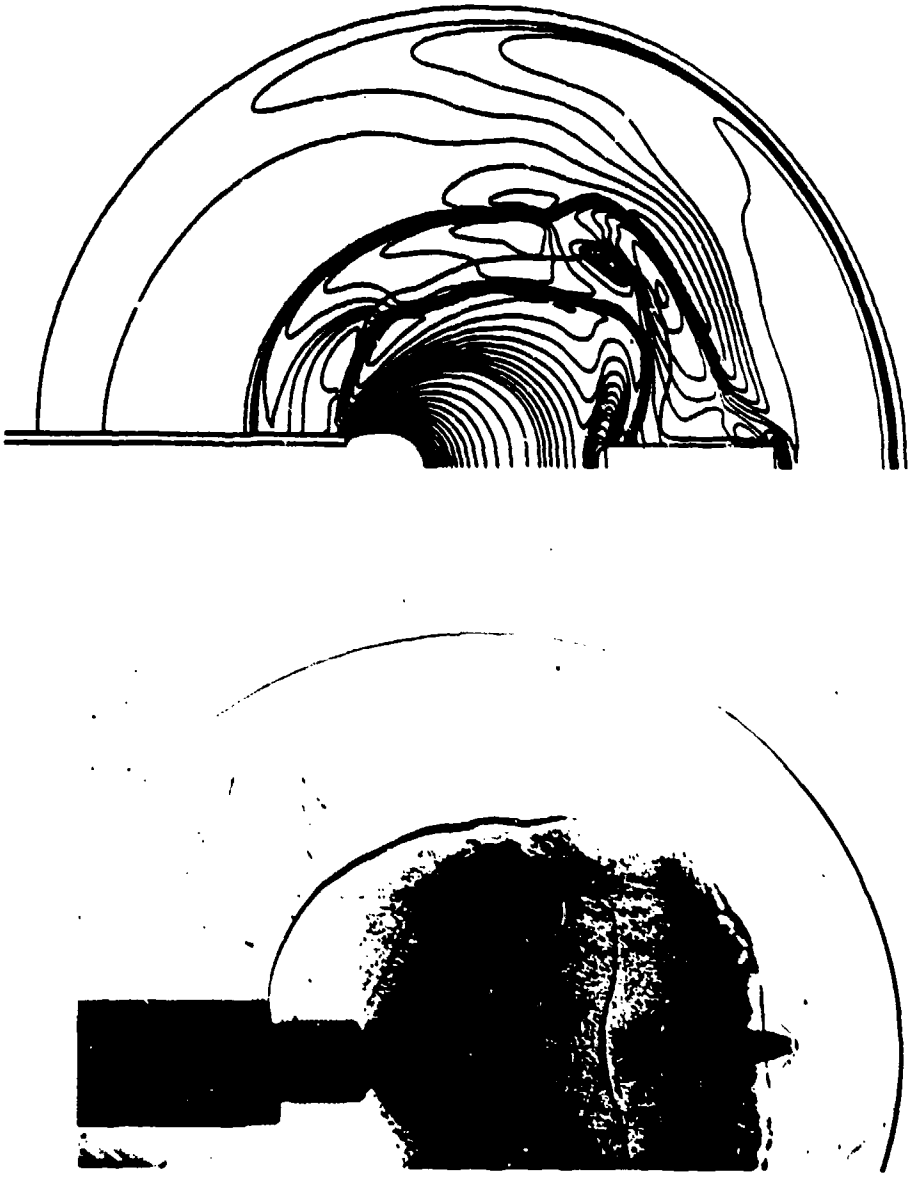

Figure A-2. Pressure contour plot and shadowgraph for the bare muzzle case, t = 0.394 msec.

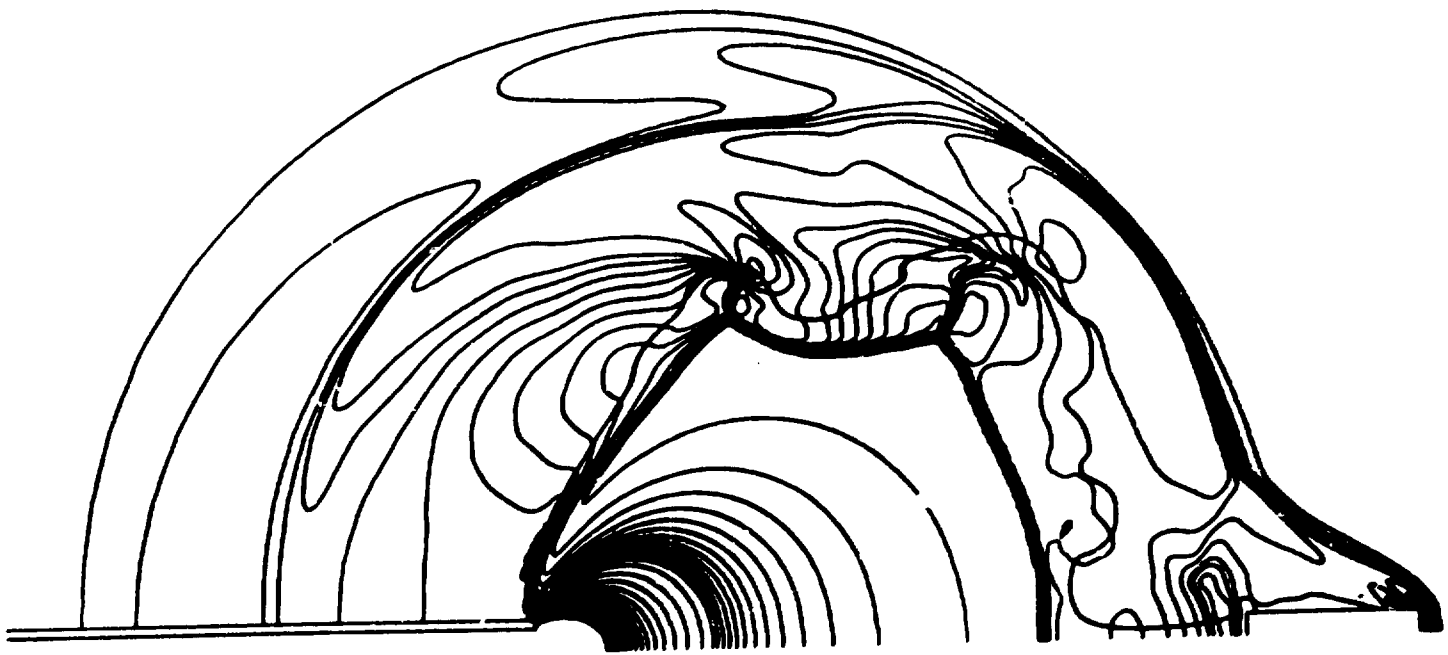

Figure A-3. Pressure contour plot for the bare muzzle case, t = 0.588 msec, corresponding to the shadowgraph in Figure A-4.

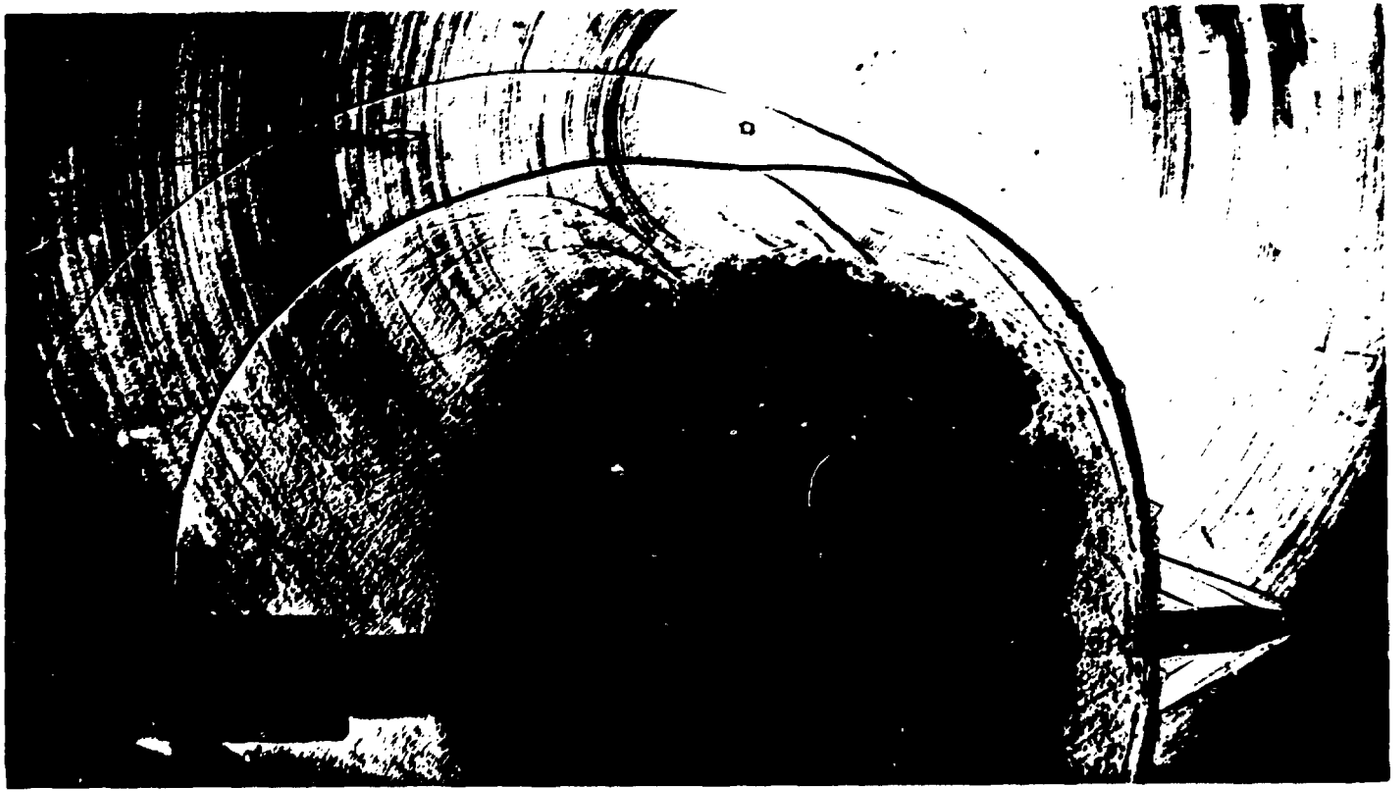

Figure A-4. Shadowgraph for the bare muzzle case corresponding to the pressure contour plot in Figure A-3.

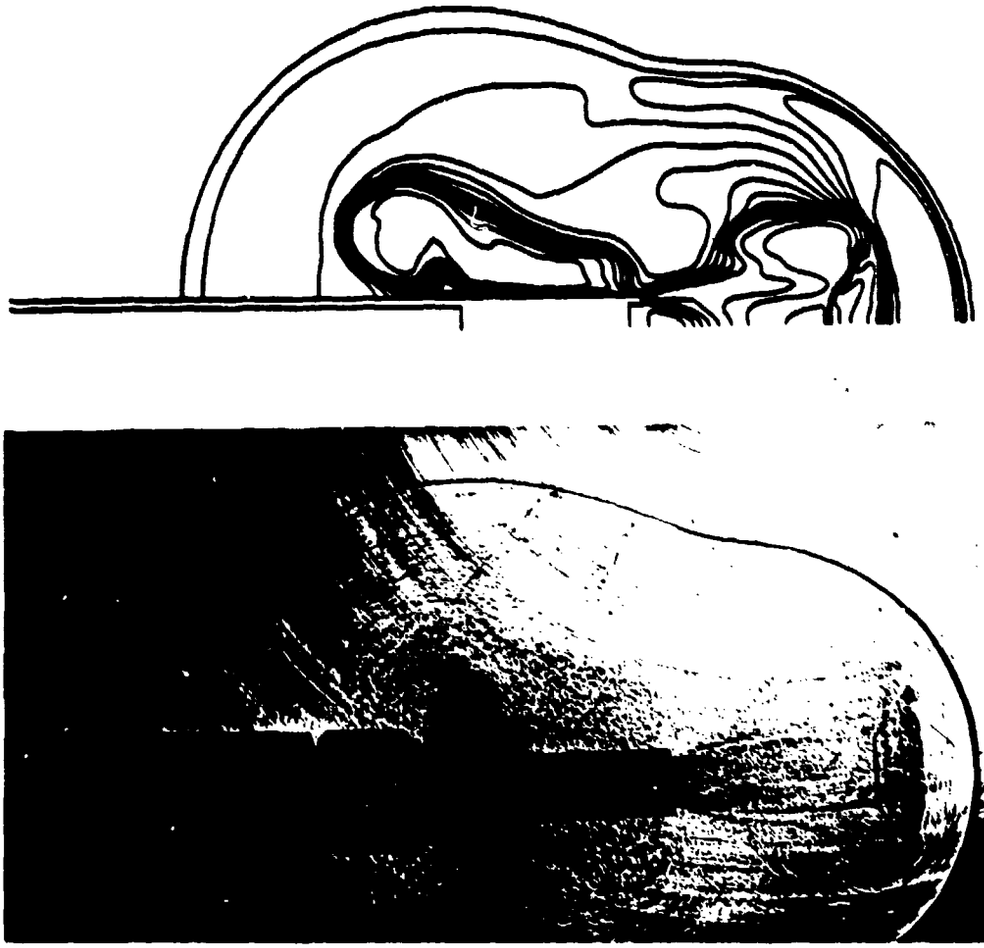

Figure A-5. Density contour plot and shadowgraph for the brake case, t = 0.315 msec.

Figure A-6. Pressure contour plot for the brake case, t = 0.584 msec, corresponding to the shadowgraph in Figure A-7.

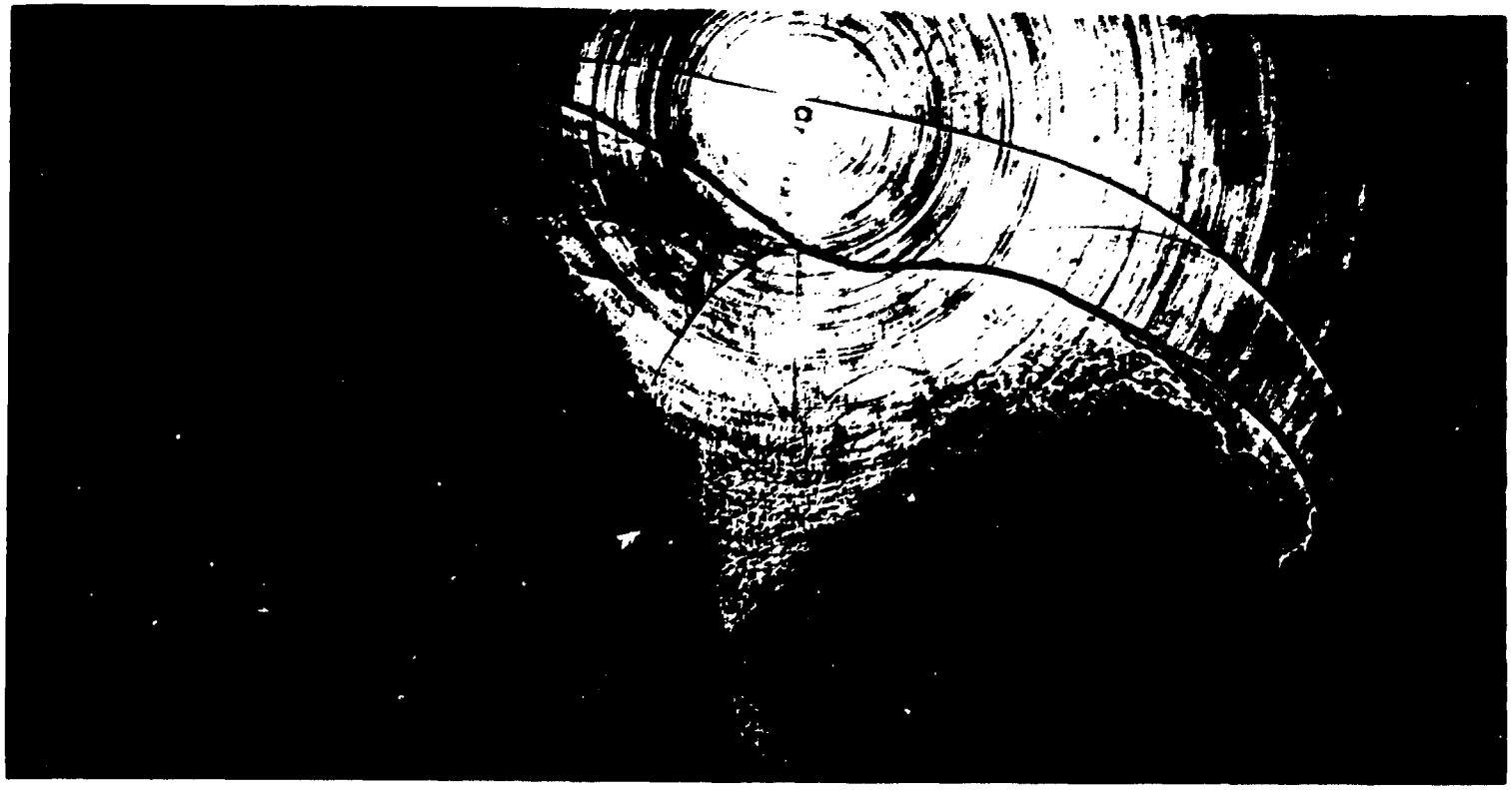

Figure A-7. Shadowgraph for the brake case corresponding to the pressure contour plot in Figure A-6.

TECHNICAL REPORT INTERNAL DISTRIBUTION LIST

	NO. OF COPIES
CHIEF, DEVELOPMENT ENGINEERING DIVISION	
ATTN: SMCAR-CCB-D	1
-DA	1
-DC	1
-DM	1
-DP	1
-DR	1
-DS (SYSTEMS)	1
CHIEF, ENGINEERING SUPPORT DIVISION	
ATTN: SMCAR-CCB-S	1
-SE	1
CHIEF, RESEARCH DIVISION	
ATTN: SMCAR-CCB-R	2
-RA	1
-RM	1
-RP	1
-RT	1
TECHNICAL LIBRARY	5
ATTN: SMCAR-CCB-TL	
TECHNICAL PUBLICATIONS & EDITING SECTION	3
ATTN: SMCAR-CCB-TL	
DIRECTOR, OPERATIONS DIRECTORATE	1
ATTN: SMCWV-OD	
DIRECTOR, PROCUREMENT DIRECTORATE	1
ATTN: SMCWV-PP	
DIRECTOR, PRODUCT ASSURANCE DIRECTORATE	1
ATTN: SMCWV-QA	

NOTE: PLEASE NOTIFY DIRECTOR, BENET LABORATORIES, ATTN: SMCAR-CCB-TL, OF ANY ADDRESS CHANGES.

TECHNICAL REPORT EXTERNAL DISTRIBUTION LIST

	NO. OF COPIES
ASST SEC OF THE ARMY RESEARCH AND DEVELOPMENT ATTN: DEPT FOR SCI AND TECH THE PENTAGON WASHINGTON, D.C. 20310-0103	1
ADMINISTRATOR DEFENSE TECHNICAL INFO CENTER ATTN: DTIC-FDAC CAMERON STATION ALEXANDRIA, VA 22304-6145	12
COMMANDER US ARMY ARDEC ATTN: SMCAR-AEE	1
SMCAR-AES, BLDG. 321	1
SMCAR-AET-O, BLDG. 351N	1
SMCAR-CC	1
SMCAR-CCP-A	1
SMCAR-FSA	1
SMCAR-FSM-E	1
SMCAR-FSS-D, BLDG. 94	1
SMCAR-IMI-I (STINFO) BLDG. 59 PICATINNY ARSENAL, NJ 07806-5000	2
DIRECTOR US ARMY BALLISTIC RESEARCH LABORATORY ATTN: SLCBR-DD-T, BLDG. 305 ABERDEEN PROVING GROUND, MD 21005-5066	1
DIRECTOR US ARMY MATERIEL SYSTEMS ANALYSIS ACTV ATTN: AMXSY-MP ABERDEEN PROVING GROUND, MD 21005-5071	1
COMMANDER HQ, AMCCOM ATTN: AMSMC-IMP-L ROCK ISLAND, IL 61299-6000	1
COMMANDER ROCK ISLAND ARSENAL ATTN: SMCRI-ENM ROCK ISLAND, IL 61299-5000	1
DIRECTOR US ARMY INDUSTRIAL BASE ENGR ACTV ATTN: AMXIB-P ROCK ISLAND, IL 61299-7260	1
COMMANDER US ARMY TANK-AUTMV R&D COMMAND ATTN: AMSTA-DDL (TECH LIB) WARREN, MI 48397-5000	1
COMMANDER US MILITARY ACADEMY ATTN: DEPARTMENT OF MECHANICS WEST POINT, NY 10996-1792	1
US ARMY MISSILE COMMAND REDSTONE SCIENTIFIC INFO CTR ATTN: DOCUMENTS SECT, BLDG. 4484 REDSTONE ARSENAL, AL 35898-5241	2
COMMANDER US ARMY FGN SCIENCE AND TECH CTR ATTN: DRXST-SD 220 7TH STREET, N.E. CHARLOTTESVILLE, VA 22901	1
COMMANDER US ARMY LABCOM MATERIALS TECHNOLOGY LAB ATTN: SLCMT-IML (TECH LIB) WATERTOWN, MA 02172-0001	2

NOTE: PLEASE NOTIFY COMMANDER, ARMAMENT RESEARCH, DEVELOPMENT, AND ENGINEERING CENTER, US ARMY AMCCOM, ATTN: BENET LABORATORIES, SMCAR-CCB-TL, WATERVLIET, NY 12189-4050, OF ANY ADDRESS CHANGES.

TECHNICAL REPORT EXTERNAL DISTRIBUTION LIST (CONT'D)

	NO. OF COPIES
COMMANDER US ARMY LABCOM, ISA ATTN: SLCIS-IM-TL 2800 POWDER MILL ROAD ADELPHI, MD 20783-1145	1
COMMANDER US ARMY RESEARCH OFFICE ATTN: CHIEF, IPO P.O. BOX 12211 RESEARCH TRIANGLE PARK, NC 27709-2211	1
DIRECTOR US NAVAL RESEARCH LAB ATTN: MATERIALS SCI & TECH DIVISION	1
CODE 26-27 (DOC LIB)	1
WASHINGTON, D.C. 20375	

	NO. OF COPIES
COMMANDER AIR FORCE ARMAMENT LABORATORY ATTN: AFATL/MN EGLIN AFB, FL 32542-5434	1
COMMANDER AIR FORCE ARMAMENT LABORATORY ATTN: AFATL/MNF EGLIN AFB, FL 32542-5434	1
METALS AND CERAMICS INFO CTR BATTELLE COLUMBUS DIVISION 505 KING AVENUE COLUMBUS, OH 43201-2693	1

NOTE: PLEASE NOTIFY COMMANDER, ARMAMENT RESEARCH, DEVELOPMENT, AND ENGINEERING CENTER, US ARMY AMCCOM, ATTN: BENET LABORATORIES, SMCAR-CCB-TL, WATERVLIET, NY 12189-4050, OF ANY ADDRESS CHANGES.